

Chromospheric imaging of the active binary system V 711 Tauri = HR 1099 in December 1992

I. Busà¹, I. Pagano^{2,3}, M. Rodonò^{1,2}, J.E. Neff⁴, and A.C. Lanzafame¹

¹ Istituto di Astronomia, Università di Catania, Italy

² Osservatorio Astrofisico di Catania, Italy

³ JILA, University of Colorado, Boulder, CO, USA

⁴ Department of Physics and Astronomy, College of Charleston, Charleston, NC, USA

Received 31 May 1999 / Accepted 26 August 1999

Abstract. Spectroscopic observations of the bright RS CVn-type system V 711 Tau = HR 1099 (K1 IV + G5 V) were obtained by IUE during the same period of a Multi-Site Continuous Spectroscopy (MUSICOS) campaign between 12–18 December 1992 (Huang et al. 1995).

We report on the results of a “Doppler Imaging” analysis of the Mg II h line. Broad, variable and extended wings have been detected and successfully fitted using a broad Gaussian, which accounts for a large fraction of flux from the global stellar Mg II h emission. This broad component is present in all spectra and presents velocity shifts with respect to the K1 star rest-frame that are variable in the range between -19 and +44 km s⁻¹. Similar results have been obtained from Doppler Imaging of the other relevant chromospheric line (H_{α}) in other RS CVn stars (c.f. Hatzes, 1995 and Hatzes, 1998). Furthermore, our analysis suggests that these shifts could be due to rotational modulation produced by an active region, that essentially straddles the pole of the K1 star in which down-flows dominate on up-flows. Finally, emitting matter between the two stars has been detected, indicating that mass-exchange is present in the binary system.

Five flare episodes with strong flux enhancements in several transition region lines were observed. These flares were preliminarily reported by Neff et al. (1995). We analyse in this paper the Mg II h and k line emission during the major of these five flare (1992 December 14), since only a weak enhancement was observed in the Mg II h and k lines during the other four flares.

Spectral imaging of the Mg II lines during this flare indicates a flaring site on the visible K1 star hemisphere with mass ejection from the K1 star towards the G5 companion. The Mg II emission shows a large broadening with FWHM reaching 1000 km s⁻¹ at flare peak and decreasing to 700 km s⁻¹ two hours after the peak.

Our analysis have been carried out using both IUESIPS and NEWSIPS processed spectra. We find that the shapes of the spectral profiles are quite different when spectra are processed by IUESIPS or NEWSIPS procedures, the IUESIPS processed spectra showing a spurious excess of flux on the red wing of the lines.

A comparison with results from GHRS-HST Mg II spectra of V 711 Tau (Dempsey et al. 1996, Wood et al. 1996) shows that, thanks to the complete phase coverage together with the improved quality obtained by the NEWSIPS reduction procedures, the bulk of information derived from GHRS data can be extracted also from the IUE spectra, which continues to be the most complete UV data set that is nowadays available on this source.

Key words: stars: activity – stars: binaries: general – stars: chromospheres – stars: flare – stars: imaging – stars: individual: V 711 Tau – stars: individual: HR 1099

1. Introduction

V 711 Tau (HR 1099, HD 22468) is one of the most active RS CVn non-eclipsing spectroscopic binary systems ($P_{rot} \approx 2^d.8$), with a G5-type component of luminosity class V and a cooler K1 IV component. The system is also the primary component of the visual binary system ADS 2644 whose secondary component is a K3 V star. V 711 Tau shows a rich variety of activity phenomena such as dark star-spots (Rodonò et al. 1986, Dorren & Guinan 1982) and highly energetic flares of order of magnitude larger than on the Sun (Linsky et al. 1989). The primary, more massive component of the close binary (the K1 star) shows very strong and variable Ca II H & K, H_{α} and ultraviolet emission that are indicative of high chromospheric activity (Rodonò et al. 1987, Neff et al. 1995, Dempsey et al. 1996, Robinson et al. 1996). Furthermore HR 1099 has been observed at radio wavelength (Owen et al. 1976, Trigilio et al. 1993, Umana et al. 1995), at soft X ray (Agrawal & Vaidya 1988), and at EUV wavelengths (Drake et al. 1994). Such high activity is strictly correlated with tidally induced synchronous rotation which makes the magnetic dynamos more efficient. Donati et al. (1990) detected, using Zeeman Doppler Imaging, a ≈ 1000 G magnetic field covering 18% of the K1 star’s surface.

In this paper, the chromospheric activity of the active binary system V 711 Tau is studied by applying a Doppler-Imaging technique to Mg II h lines. In Sect. 2 we present the observations and data reduction. The Doppler Imaging technique is described

Send offprint requests to: I. Busà

Correspondence to: ebu@sunct.ct.astro.it

Table 1. Properties of the close binary system V 711 Tau (=HR 1099)

Sp. type ^a	K1 IV	G5 V	
Temperature ^b	4750	5450	K
Radius ^a	3.9±0.2	1.3±0.2	R _⊙
Mass ^a	1.4±0.2	1.1±0.2	M _⊙
$v \sin i^b$	38±1	13±1	km s ⁻¹
M _v ^a	3.7	4.2	
K ^c	50.0±0.5	62.8±0.6	km s ⁻¹
γ^c		-15.4±0.3	km s ⁻¹
$a \sin i^a$	1.93±0.02	2.41±0.02	10 ⁶ km s ⁻¹
M sin ³ i	0.224±0.005	0.180±0.004	M _⊙
i^a		33±2	degree
e^a		0.014±0.099	
P _{orb} ^a		2.83774±0.00001	day
HJD ₀ ^b		2442766.080	
d ^e		28.98	pc

^a Fekel, 1983^b Vogt & Penrod, 1983^c Donati et al. 1992^d Strassmeier et al. 1993^e Hipparcos Catalogue

in Sect. 3.1.1. The imaging results for the quiescent and flaring phase are discussed in Sect. 3. The conclusions are drawn in Sect. 4.

2. Observations and data reduction

Ultraviolet observations of V 711 Tau were obtained by the IUE satellite over 6 days from 12 to 18 December 1992 during a Multi-Site Continuous Spectroscopic (MUSICOS) campaign (Huang et al. 1995). The data set consists of 76 high-dispersion LWP spectra of the Mg II *h* (2803.53 Å) and *k* (2796.35 Å) lines, covering more than two contiguous orbital/rotational periods. We have analysed both the spectra reduced using the IUESIPS (IUE Spectral Image Processing System) procedure (cf. also Busà et al. 1996), and the subsequent Final Archive spectra reduced by the NEWSIPS (New Spectral Image Processing System) procedure. We discuss in Sect. 3.3 the results of the NEWSIPS data analysis, and comment on the difference between the NEWSIPS and IUESIPS results.

Orbital phases were computed using the ephemeris HJD 2,442,766.080 + 2.83774E (Strassmeier et al., 1993), with an accuracy $\Delta\phi = 0.01$.

The physical characteristic and orbital elements of V 711 Tau are listed in Table 1.

The spectral resolution is about 0.2 Å for the Mg II region. The instrumental profile is Gaussian with FWHM=0.25 Å. Since the Mg II *k* line was saturated in most of the IUESIPS spectra, we have concentrated our analysis on the Mg II *h* line. However, the NEWSIPS reduction removed the saturation in the core of the *k* line (see Sect. 3.3), allowing us to measure the ratio between the *h* and *k* lines that is 0.80±0.08. It is worth noting that the ratio between the *h* and the saturated *k* lines in IUESIPS data is 0.79±0.06, implying that the saturation effect, in the *k*

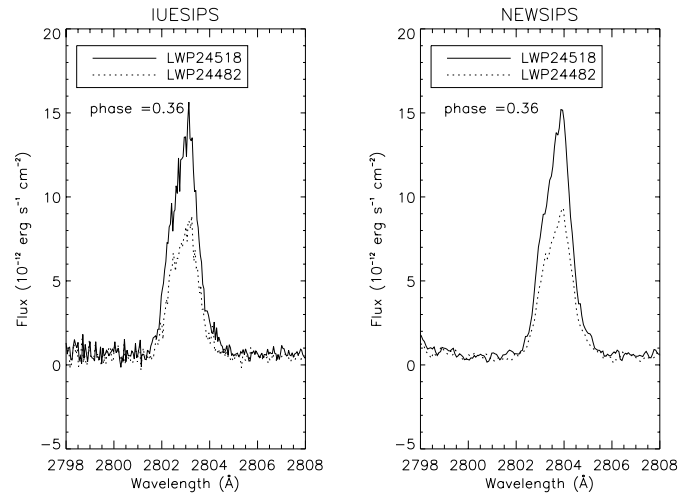


Fig. 1. Comparison between spectra obtained at the same phase, the lower spectrum (LWP24482) in coincidence with a scattered light background peak (*left panel*: IUESIPS reduction; *right panel*: NEWSIPS reduction). It is evident that the NEWSIPS procedure reduction improves the quality of the spectra, but does not solve the flux calibration problem in presence of scattered light.

line core, was not too severe in the IUESIPS and that only a few spectra were actually affected. A summary of the observations is given in Table 2. For unknown reasons the high-dispersion spectra LWP24464, LWP24481, LWP24496 have been degraded to low-dispersion in the NEWSIPS reduction procedure, and, therefore, these spectra were not included in the present high-resolution study. The NEWSIPS spectra LWP24499 and LWP24538 show peculiar flux drops which were not present in the original IUESIPS data. Therefore, these spectra have been discarded as well. Finally, the NEWSIPS spectra LWP24466, LWP24467, LWP24482, LWP24494, LWP24495, LWP24520 and LWP24530 have been discarded because, as IUESIPS spectra (see Neff et al., 1992), they are obviously affected by scattered light, and the flux calibration leads to “drop outs” in coincidence with scattered light background peaks. The NEWSIPS reduction does not appear to have improved this calibration problem (see Fig. 1, as a representative example).

In Fig. 2 the Mg II *h* fluxes, integrated between 2798 and 2808 Å, are plotted versus the orbital phases. Random variability of the integrated flux is evident, but no rotational modulation is visible. Marked enhancement in several transition region UV lines have been detected during the monitoring time at phases $\phi = 0.84, 0.97, 0.18, 0.55$, and 0.89, listed in order of acquisition time (see Neff et al. 1995). Of these flaring episodes, the flare at $\phi=0.55$ during the second orbit (LWP24490 spectrum on Dec 14 at 10:30 UT) shows the most marked flux enhancement of the Mg II line emission.

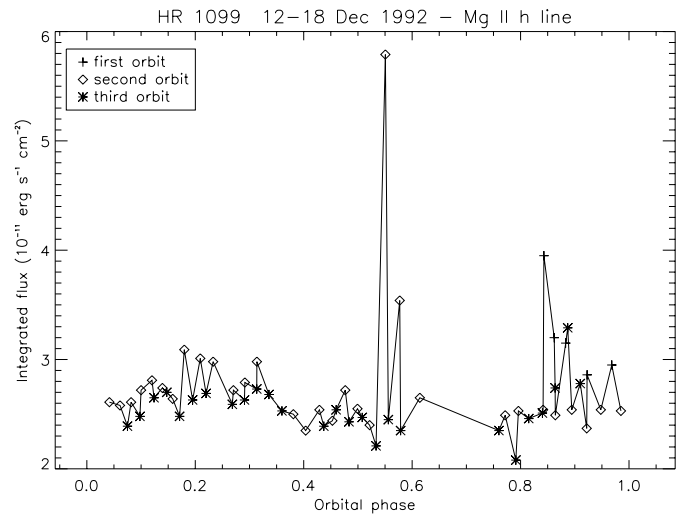
In Fig. 3 the Mg II *h* line profile at $\phi = 0.27$ (when the component stars are at their maximum separation) is shown. Arrows mark the expected radial velocities of the G5 and K1 stellar components. The composite line profile is strongly asymmetric indicating that the emission flux from the G5 star is weaker than from the K1 star.

Table 2. Summary of IUE observations

Image	Date	Start at UT	Exp. (s)	Phase mid exp
24460	1992 Sep 12	10:08:16	1200	0.84
24461	1992 Sep 12	11:25:52	1200	0.86
24462	1992 Sep 12	12:53:36	1080	0.88
24463	1992 Sep 12	15:34:55	1080	0.92
24464	1992 Sep 12	17:15:00	1200	0.95
24465	1992 Sep 12	18:40:04	1200	0.97
24466	1992 Sep 12	20:21:24	1200	0.99
24467	1992 Sep 12	21:54:34	1200	0.02
24468	1992 Sep 12	23:37:16	1500	0.04
24469	1992 Sep 13	00:57:26	1500	0.06
24470	1992 Sep 13	02:20:54	1500	0.08
24471	1992 Sep 13	03:35:50	1500	0.10
24472	1992 Sep 13	04:58:19	1500	0.12
24473	1992 Sep 13	06:16:28	1500	0.14
24474	1992 Sep 13	07:34:48	1500	0.16
24475	1992 Sep 13	09:01:52	1500	0.18
24476	1992 Sep 13	11:02:25	1500	0.21
24477	1992 Sep 13	12:39:00	1500	0.23
24478	1992 Sep 13	15:11:49	1500	0.27
24479	1992 Sep 13	16:38:16	1500	0.29
24480	1992 Sep 13	18:06:22	1800	0.31
24481	1992 Sep 13	19:27:27	1800	0.33
24482	1992 Sep 13	21:11:18	1800	0.36
24483	1992 Sep 13	22:36:28	2400	0.38
24484	1992 Sep 14	00:09:22	2400	0.40
24485	1992 Sep 14	01:52:38	2400	0.43
24486	1992 Sep 14	03:30:34	2400	0.45
24487	1992 Sep 14	05:09:51	2100	0.48
24488	1992 Sep 14	06:40:00	2400	0.50
24489	1992 Sep 14	08:11:07	2400	0.52
24490	1992 Sep 14	10:09:57	2400	0.55
24491	1992 Sep 14	11:58:18	2400	0.58
24492	1992 Sep 14	14:29:53	2400	0.61
24493	1992 Sep 14	16:08:27	2400	0.64
24494	1992 Sep 14	18:12:56	2400	0.67
24495	1992 Sep 14	20:02:55	1575	0.69
24496	1992 Sep 14	23:24:48	2400	0.74
24497	1992 Sep 15	01:13:08	2400	0.77
24498	1992 Sep 15	02:52:34	2400	0.80
24499	1992 Sep 15	04:31:41	2100	0.82
24500	1992 Sep 15	06:01:00	2100	0.84
24501	1992 Sep 15	07:31:03	2400	0.86
24502	1992 Sep 15	09:35:00	2400	0.89
24503	1992 Sep 15	11:27:47	2400	0.92
24504	1992 Sep 15	13:13:50	2400	0.95
24505	1992 Sep 15	15:55:36	1200	0.98
24506	1992 Sep 15	21:52:39	2400	0.07
24507	1992 Sep 15	23:26:23	2400	0.10
24508	1992 Sep 16	01:12:46	2400	0.12
24509	1992 Sep 16	02:48:51	2400	0.15
24510	1992 Sep 16	04:25:23	2400	0.17
24511	1992 Sep 16	06:03:36	2400	0.19
24512	1992 Sep 16	07:45:12	2400	0.22
24514	1992 Sep 16	11:08:22	1800	0.27
24515	1992 Sep 16	12:39:13	1800	0.29
24516	1992 Sep 16	14:12:02	1800	0.31

Table 2. (continued)

Image	Date	Start at UT	Exp. (s)	Phase mid exp
24517	1992 Sep 16	15:43:35	1800	0.34
24518	1992 Sep 16	17:16:51	2400	0.36
24519	1992 Sep 16	19:03:19	2400	0.39
24520	1992 Sep 16	20:38:49	2100	0.41
24521	1992 Sep 16	22:32:40	2400	0.44
24522	1992 Sep 17	00:05:20	2400	0.46
24523	1992 Sep 17	01:42:20	2400	0.48
24524	1992 Sep 17	03:21:47	2400	0.51
24525	1992 Sep 17	05:08:32	2100	0.53
24526	1992 Sep 17	06:41:19	2100	0.56
24527	1992 Sep 17	08:13:35	2100	0.58
24530	1992 Sep 17	18:57:40	1800	0.74
24531	1992 Sep 17	20:32:5	2400	0.76
24532	1992 Sep 17	22:39:41	2400	0.79
24533	1992 Sep 18	00:17:06	2400	0.81
24534	1992 Sep 18	02:00:16	2400	0.84
24535	1992 Sep 18	03:35:49	2400	0.86
24536	1992 Sep 18	05:11:22	2400	0.89
24537	1992 Sep 18	06:45:46	2400	0.91
24538	1992 Sep 18	08:20:16	1680	0.93

**Fig. 2.** Integrated Mg II *h* line flux versus orbital phase. See text for details.

The spectra were fitted adopting Gaussian profiles. We used the “ICUR Spectral Analysis Package” fitting program (version 3.1) based upon CURFIT (Bevington, 1969), which uses the Marquadrat algorithm to minimise the χ^2 .

3. Results

We have separated our analysis into the non flaring and flaring states. In the study of the non-flaring state we have discarded all the spectra affected by the flares occurring at orbital phases 0.84 and 0.97 in the first orbit, 0.18 and 0.55 in the second orbit and 0.89 in the third orbit. Therefore, the analysis of the “quiescent” states involves only spectra acquired during the 2nd and 3th or-

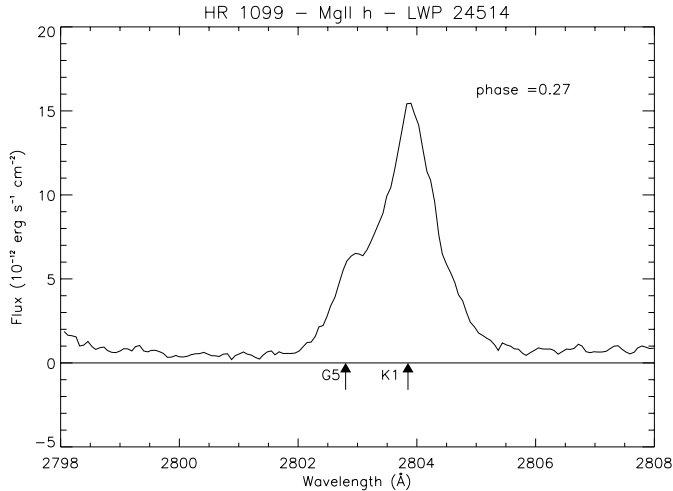


Fig. 3. The Mg II h line profile at $\phi = 0.27$ when the K1 and G5 stars are at their maximum separation. Arrows indicate the expected central wavelengths of the Mg II h lines from the two stars.

bits. As far as the flare states are concerned, we discuss in detail only the major flare whose peak was observed on December 14 at 10:30 UT (phase 0.55).

3.1. Non flaring state

3.1.1. Method

The analysis of the non flaring phase is based upon the *Doppler Imaging Technique*. The *Doppler Imaging* is an observational and computational technique that uses a series of high-resolution spectral line profiles to produce a map of the stellar surface (Vogt et al. 1987, Bruls et al. 1998, Strassmeier & Rice, 1998). In the spectrum of a very rapidly rotating star, there is a correspondence between the wavelength of a narrow spectral feature, either in emission or absorption, moving over the rotationally broadened profiles of a spectral line and the spatial position of a compact feature on the stellar disk. Due to this correspondence, a feature that traverses the visible stellar disk can produce a bump or a dip that moves across the observed profile. Note that the phase interval during which a given spectral feature is visible on a broad line profile is 0.5 for an equatorial feature, while a polar feature is, at least in part, always visible. The decomposition of the spectra into components provides information on the structure of the stellar surface. A schematic description of the technique can be found in Vogt & Penrod (1983).

In this paper the decomposition of the spectra is based on the identification of the following components:

- the *quiet emission*, i.e. outside of flaring state, of K1 and G5 stars;
- the absorption due to the ISM;
- the *short-term variable component*;
- additional components due to extra emissions with respect to the quiet emission;

For each star, we define *quiet emission* the highest emission compatible with a uniform (over the stellar surface - single orbit) and constant (over the two orbits included in the data set) contribution to the total emission. Such quiet emission must, therefore, be symmetric with respect to the central wavelength of the star and be present at all phases.

In order to measure a quantitative value of the quiet emission we have fitted the whole set of spectra using, at first, a three Gaussian fit: two components to fit the stellar emission, and a third component to fit the interstellar medium (ISM) absorption. The central wavelengths of two Gaussian components have been placed at the expected radial velocities of the K1 and G5 stars. For the third component we have assumed an instrumental profile FWHM of 0.25 \AA representing the unresolved ISM absorption line.

The fits of spectra acquired at phases close to conjunctions obviously poses serious deconvolution problems. In order to overcome such difficulties, we have constrained the flux and width of the quiescent components using the fits obtained close to quadratures. Therefore, we have used an iterative procedure to refine the most likely flux and width of the quiet emissions from each star, first fixing the flux and using the width as a free parameter, then fixing the width and using the flux as a free parameter. Finally, the highest possible emission compatible with the above constraints have been sought. The procedure was repeated imposing that the quiet flux did not vary more than the estimated *short term variability* (see below) from one spectrum to the next and that the line width does not vary more than three times the accuracy on the velocity, until consistency is reached for all spectra. The flux and width so obtained are then used as most likely values (first guess) for the successive analysis.

The standard deviation of flux differences between spectra obtained almost at the same phase in two contiguous orbits is taken as both an index of the *short term variability* and as uncertainty on the quiet emission flux.

This initial approach readily showed us that most of the spectra could not be accurately fitted by only three Gaussian components.

The extra components required to get a reasonable agreement between the observed spectrum and the sum of the two quiet emission components and the ISM absorption component were interpreted as possibly due to discrete emitting regions (active areas). The identification of such extra components has been aided by consistency with the geometry of the binary system and with the temporal evolution of the active region.

After the identification of the emitting components, the location on the star surface of discrete emitting regions was done according to Neff et al. (1989).

3.1.2. Doppler imaging results

Fig. 4 shows four representative fits of the spectra acquired at phases 0.27 during the second and third orbit, and at phases 0.51 and 0.76 during the third orbit. Note that the stellar quiet emission components are not fully separated even close to the quadratures (phases 0.27 and 0.76). The ISM absorption com-

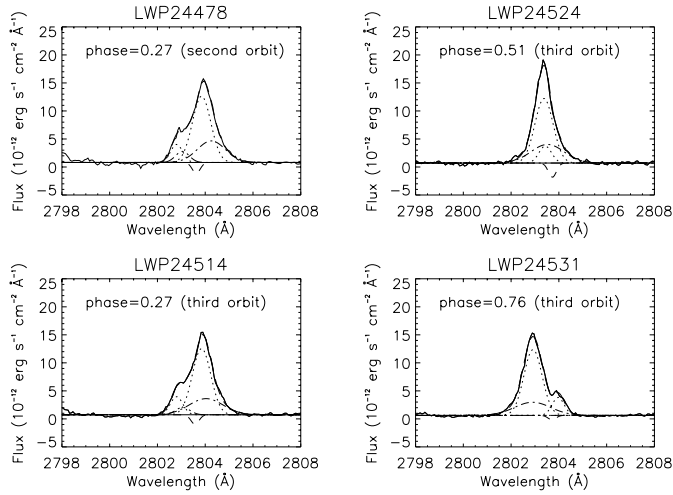


Fig. 4. Representative fits of the Mg II h lines of V 711 Tau. The *quiet emission* from the two star and the ISM absorption are drawn with dotted lines. The additional emission components are drawn with dot-dashed lines. The continuous lines show the final fits.

Table 3. Mean integrated flux and FWHM from the quiet emissions of the K1 and G5 stars.

	K1 star	G5 star	
Flux	11.1 ± 0.5	2.3 ± 0.2	$10^{-12} \text{ erg cm}^{-2} \text{ s}^{-1}$
FWHM	89.7 ± 2.1	52.5 ± 2.6	km s^{-1}

ponent is stable in central wavelength and equivalent width, as expected. To fit the variables and extended broad wings of the Mg II h profiles, a broad Gaussian, which accounts for a large fraction of flux from the stellar Mg II h emissions, was required for all the analysed spectra. Between phase 0.1 and 0.4 a further component, much narrower than the broad component, was required to get acceptable fits.

From the final fit the Gaussian components representing the quiet emission of the two stars are approximately constant, this supports the validity of the solution we found. The shape and strength of the broad and narrow components vary, maintaining approximately their line width and peak intensity from one rotation to the next (e.g. at $\phi = 0.27$ of the second and third orbit, respectively).

From the central wavelength of the ISM line, we have calculated that the ISM in the direction of HR 1099 has a velocity $v_{IS} = 19 \pm 6 \text{ km s}^{-1}$. This value is in agreement with the $v_{IS} = 23 \pm 7 \text{ km s}^{-1}$ measured by Anderson & Weiler (1978) and with the $v_{IS} = 21.9 \pm 0.06 \text{ km s}^{-1}$ measured by Piskunov et al. (1997). The EW_{IS} is constant with a value of $62.3 \pm 14.5 \text{ mÅ}$. Dempsey et al. (1996) using GHRS Mg II spectra resolve the ISM absorption in three discrete components. The measured velocities for the three components are +7.3, +14.5 and +21.7 km s^{-1} , and the corresponding equivalent widths are 10, 30, and 40 mÅ.

By comparing the spectra obtained at the same phase and different orbits, we have observed that their Mg II h integrated flux never differ for a value higher than $2 \times 10^{-12} \text{ erg cm}^{-2} \text{ s}^{-1}$.

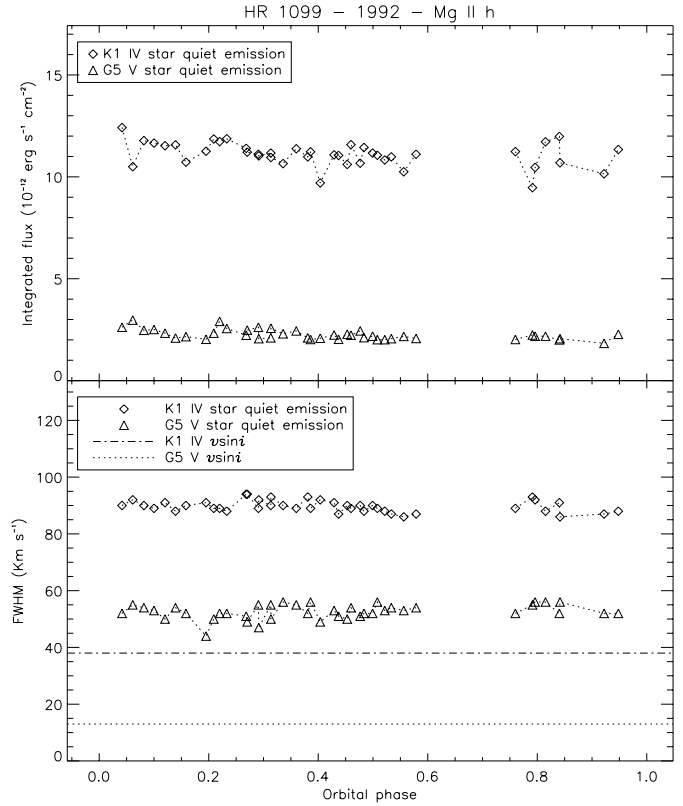


Fig. 5. Integrated fluxes (*top panel*), and FWHM (*bottom panel*) of the quiet emission from G5 and K1 stars.

We have assumed this value as a good estimate of the mean short term variability.

3.1.3. Quiet emission components

The quiet emissions of the two components of the binary system were found by iterative decompositions of the observed spectra, as discussed in Sect. 3.1.1. An important constraint comes from spectra obtained close to phases 0.25 and 0.75. The values found at these phases were adopted as upper limits to the quiet components fluxes. Because of short-term variability, in the final fits the integrated flux due to the quiet emission was estimated allowing it a maximum variation of $\pm 2 \times 10^{-12} \text{ erg cm}^{-2} \text{ s}^{-1}$. The FWHM of the quiet components were estimated allowing a maximum variation of three times the accuracy on the velocity (6 km s^{-1}).

The mean integrated flux and FWHM of the G5 and K1 quiet emissions are listed in Table 3 and are plotted versus phase in Fig. 5.

The Wilson-Bappu relation given by Elgarøy et al. (1997), $M_v = 37.34 - 19.13 \log W$, where W is the FWHM of the Gaussian that fit the Mg II h line and M_v is the visual absolute magnitude of the star, predicts line widths of 54 km s^{-1} and 57 km s^{-1} , for the G and K stars, respectively. While the FWHM of the G star quiet emission agrees quite well with the predicted Wilson-Bappu value, the FWHM of the K star quiet emission is $\sim 58\%$ greater than predicted by the Wilson-Bappu

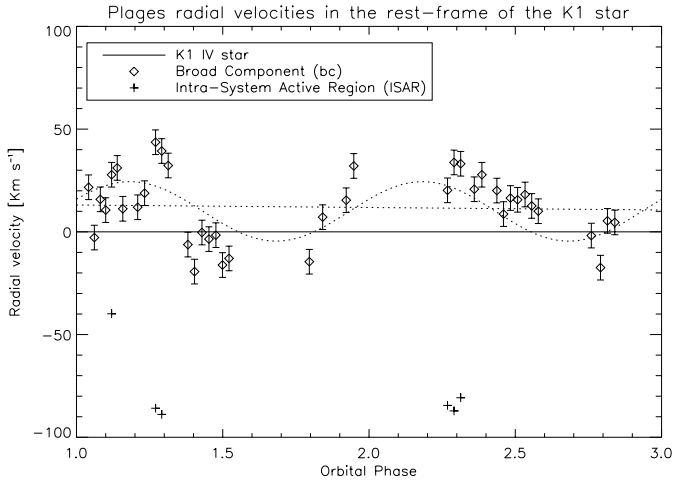


Fig. 6. Radial velocities of the additional Gaussian components resulting from the spectral decomposition of the Mg II *h* line profiles. The error bars are 1σ standard deviations. The dotted lines are the best fits, linear and sinusoidal, to the radial velocities of the broad Gaussian component associated to the K1 star (*diamonds*).

relation. This fact is in agreement with the result obtained by Elgarøy et al. (1997) that stellar activity affects the line widths and that the Wilson-Bappu relation should be modified to add an activity-related term to the fundamental parameters that determine the line width, namely gravity, effective temperature and metallicity. Other cases of inconsistent stellar data with those predicted by Wilson-Bappu effect are discussed by Ayres (1980).

3.1.4. Discrete emitting regions

We have fitted the residuals between the quiet emission (including the ISM absorption) and the observed spectra by means of one or two Gaussian (see Fig. 4) components. We find that a broad component, that accounts for most of the residual flux, is required at all phases to fit the broad and extended wings of the Mg II *h* profiles. Between phases 0.1 and 0.4 it was necessary to add an extra, though small, component in order to obtain a satisfactory fit. The integrated fluxes and FWHM of additional components are shown in Fig. 7. The radial velocities of the broad Gaussian component, together with the radial velocities of the extra component found between phases 0.1 and 0.4 are plotted in Fig. 6 versus phase in the rest frame of the K1 star.

The broad component is generally red-shifted with respect to the K1 star, although the amount of red-shift is highly variable from one phase to the other. The mean value of the broad component shift is $+12 \pm 6 \text{ km s}^{-1}$, with a maximum blue-shift of -19 km s^{-1} and a maximum red-shift of 44 km s^{-1} .

The transition region lines of several RS CVn-type stars, main sequence and giant stars show broad wings (Wood et al. 1997). This phenomenon was observed for the first time on the M dwarf star AU Mic by Linsky & Wood (1994), who modelled the profiles of the C IV 1548.2 Å, 1550.8 Å and Si IV 1393.4 Å, 1402.8 Å doublets with a narrow plus a broad emission compo-

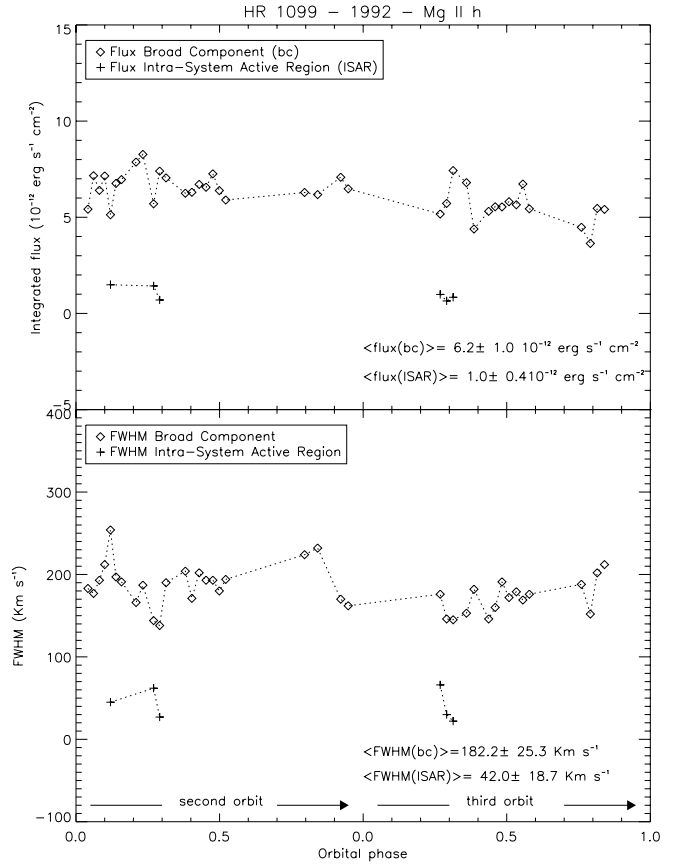


Fig. 7. Integrated fluxes (*top panel*) and FWHM (*bottom panel*) of the broad Gaussian component (*bc*) associated to the K1 star.

nent. Wood et al. (1997) showed that the narrow components can be produced by turbulent wave dissipation or Alfvén wave heating mechanisms, while the broad components are good diagnostics of microflare heating. In fact, the broad components are reminiscent of the broad C IV profiles observed in solar transition region explosive events (CME, see Dere et al. 1997), which are thought to be associated with emerging magnetic flux regions where field reconnection occurs.

Other stars also show different velocity shifts of the broad and narrow components in transition region lines. For example, β Cet (K0 III) shows 13 km s^{-1} red-shift, 31 Com (G0 III) shows 8 km s^{-1} blue-shift, and β Dra (G2 Ib-II) shows no shift, 8 km s^{-1} blue-shift, and 8 km s^{-1} red-shift at 3 different epochs (cf. Wood et al. 1997). However, all these measurements were derived from single spectra or spectra obtained at a few orbital phases. Our data, acquired at many phases during two complete stellar orbits, show that the broad component has a velocity shift that rapidly changes in time. Hence, we have the possibility of checking whether these observed velocity changes could be attributed to rotational modulation effects.

We have attempted to interpret the observed velocity variations of the broad component as due to emission arising from a localised region on the stellar chromosphere. To this purpose, we have fitted the radial velocities of this component with a sinusoidal curve.

In fact, an active region localised at latitude l and longitude L on the stellar surface causes a relatively narrow emission feature superimposed on the line profile and its velocity shift with respect to the line centroid can be represented by a sinusoidal curve:

$$V = v \sin \hat{i} \cos l \sin(2\pi\phi + L) \quad (1)$$

where ϕ is the orbital phase.

In order to estimate the error on the radial velocities of the broad component, which has to be taken into account in the sinusoidal fit, we have repeated several times the fit procedure, constraining each time the parameters of the quiet emission Gaussians to assume different values in the range of the acceptable variation as defined in Sect. 3.1.3. We find a 1σ error of 6 km s^{-1} which coincides with the typical radial velocity accuracy of IUE measurements.

We find that a sinusoidal curve (see the sinusoidal dotted line in Fig. 6) does not seem to be a good representation of the observed velocities of the broad component ($\chi^2=5.4$, for a typical $\sigma = 6 \text{ km s}^{-1}$). However, this large χ^2 value might not be so discriminant if we take into account that the broad component contains most of the flux variability that the system manifests during non-flaring phase, that is, it contains the highly variable emissions from a possibly random distribution of microflaring regions and chromospheric variability in general. Furthermore, the broad component is often overlapped with the other component revealed only between phases 0.1 and 0.4, while should also be detectable between phases 0.6 and 0.9. Finally, an hypothetical inhomogeneity localised on the surface of the K1 star could have a short-time evolution which, together with the previous factors, contributes to shift the centroid of such an inhomogeneity emission. For comparison we have tried to fit the radial velocities also by a linear function, and we find that such a linear fit (see the dotted line in Fig. 6) leads to a larger $\chi^2=7.7$. We retain the better agreement of the data with a sinusoidal fit rather than with the linear fit, together with the above considerations, indicates that the excess emission represented by the broad component is localised, at least in part, on an active region.

The sinusoidal curve that best fits the broad component radial velocity in the rest frame of the K1 star corresponds to $L=0.102 \text{ rad}$ and $v \sin \hat{i} \cos l = 15$ in Eq. (1). Such a curve describes the motion of a plage located at latitude $> 67^\circ$ and longitude $\approx 0^\circ$ on the surface of the K1 star, under the assumption that the system rotates rigidly. An additive constant shift of 10 km s^{-1} has been required by the fit, indicating that the broad component is also red-shifted of about 10 km s^{-1} , on the average, with respect to the central rest wavelength of the K1 star. This red-shift could be the effect of a circulation system in which the downward leg of the flow pattern produces most of the line emission. A similar modulation of a chromospheric line (H_α) was found by Hatzes (1998) on HD 106225, who interpreted it as arising from a plage located at high latitude and spatially related to photospheric almost polar spots.

Also Wood et al. (1996) revealed the presence of broad wings in the chromospheric Mg II resonance lines of V 711 Tau. These authors performed multi-Gaussian fits to one Mg II line

profiles in GHRS-HST spectra and found that the fit of the K1 star emission requires one narrow and one broad component. Both components are slightly red-shifted with the k line showing the largest shift. The fits also suggest that the broad component is more red-shifted than the narrow component, and that the broad component accounts for the majority of the line flux. Wood et al. (1996) concluded that although the Mg II profiles are mainly dominated by opacity effects, the modelling of extended wings requires the presence of high turbulence (e.g. microflaring) in the emitting plasma.

Also Dempsey et al. (1996) detected variable and extended wings in four GHRS-HST Mg II spectra of V 711 Tau. They found that the broad wings were symmetric with respect to the K1-star radial velocity and that much of the observed variability could be attributed to changes in the line wings. These authors, after subtracting the ISM absorption and the 2798 \AA emission components (the latter is not resolved in the IUE spectra), were able to fit a three-Gaussian model to the GHRS Mg II spectra; one narrow Gaussian component for each star, plus a broad Gaussian component associated with the K1 star.

Dempsey et al. (1996) posed the question if the extended wings of the Mg II h and k profiles are related with flares and whether they disappear during quiescent phases. In fact, the spectra that these author have analysed were acquired during a period of significant flaring, and the detection of broad wings in other stars (Linsky & Wood 1994, Linsky et al. 1995, Wood et al. 1996) comes from single-epoch observations for which the state of the system, if flaring or quiescent, was unknown.

Both Wood et al. (1996) and Dempsey et al. (1996), from the analysis of transition region lines of V 711 Tau found that most of the lines observed at $\phi = 0.24$ were blue-shifted, whereas almost all of the lines observed at the opposite quadrature $\phi = 0.64-0.67$ were red-shifted relative to the K1 star. They interpreted this fact as due to having ignored the G5 star's flux contribution in the fit. However, the phase related variation of the velocity shifts found by these authors could be also compatible with the presence of an active region that induce a variation in the line centroid position as the star rotates.

Our analysis of the IUE spectra confirm that the Mg II lines due to the K1 star of V 711 Tau can be represented by a narrow component, that in our study has been identified as the quiet emission component, plus a broad component that is present at all phases. Recent STIS-HST observations confirm the presence of transition region broad wings on the M dwarf star AU Mic during quiescence (Pagano et al. 1999), in agreement with our results on V 711 Tau.

On the basis of the results obtained by Pagano et al. (1999), Wood et al. (1997), Wood et al. (1996) and Dempsey et al. (1996), we argue that the broad component found in our analysis represents the emission of chromospheric regions with different physical conditions (most probably both high turbulence and high density) with respect to the quiescent background. Moreover, our complete phase coverage suggests that these peculiar conditions refers only to a discrete region and not to the whole chromosphere of the K1 star. Such a hypothesis is in agreement with the activity-broad-component correlation found by Wood

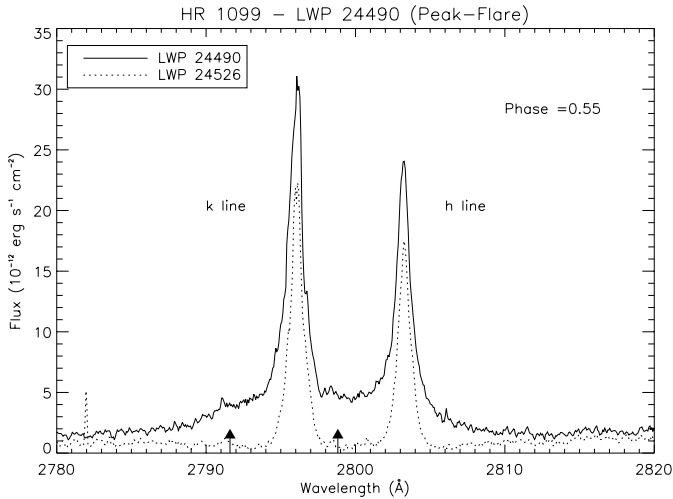


Fig. 8. LWP 24490 spectrum in the region of the Mg II *h* & *k* lines, acquired on December 14 at 10:30 UT (phase=0.55) during a flare peak, compared with the LWP 24526 spectrum acquired during quiescence at the same phase one orbit later. Arrows indicate the Mg II 3d-3p lines.

et al. (1997). Furthermore, the spatial configuration of the chromospheric inhomogeneities, resulting from our study is very similar to the stable photospheric spots configuration observed from 1981 to 1992 on V 711 Tau (see Rodonò et al. 1986, Vogt et al. 1999). It is worthwhile to mention that also the H_{α} profile of several RS CVns requires a constant narrow and a highly variable broad component to be reproduced (see for example Hatzes 1995).

We conclude that our results carried on the Mg II NEWSIPS spectra are in general agreement with Wood et al. (1996) and Dempsey et al. (1996) analysis, but our complete phase coverage allows us to infer additional information on the surface structure of the K1 component of V 711 Tau that were not possible to obtain from the phase-limited GHRS Mg II data sets.

Assuming that the binary system rotates rigidly, the additional emission components found between phases 0.1 and 0.4 (see cross points in Fig. 6) can be due to the presence of hot emitting matter at $2.9 R_{\odot}$ from the centre of mass of the system, on the G5 star side. This component should be visible also between phases 0.6 and 0.9, but in this range it is blended with the broad dominant component and it is not possible to resolve it (the averaged emitted flux of this component is only $\approx 14\%$ that of the broad component). The presence of an intra-system active region (ISAR) may be due to mass exchange from the K1 towards the G5 star. The Lagrangian point L_1 is, in fact, only $0.5 R_{K1}$ above from the photosphere of the K1 component. Note that Buzasi et al. (1991) have observed phenomena that they interpret as mass exchange with an accretion rate for the G5 star of $10^{-12} M_{\odot} \text{ year}^{-1}$.

3.2. Flaring state

Five flare episodes were observed on HR 1099 during the monitoring time as reported in Neff et al. (1995), who analysed the temporal evolution of several chromospheric and transition re-

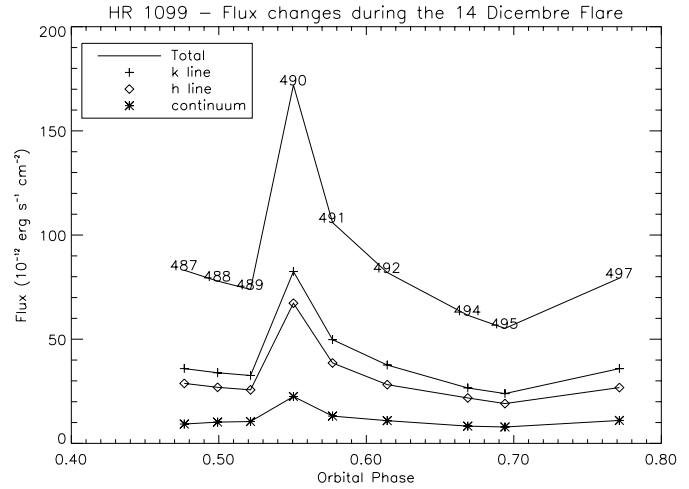


Fig. 9. Integrated flux in Mg II lines of V 711 Tau spectra collected close to the second orbit flare at $\phi = 0.55$. Numbers indicate LWP images -24,000.

gion lines. However, the Mg II *h* & *k* emission lines increased dramatically only during the flare observed on December 14 at 10:30 UT i.e. at $\phi=0.55$ of the 2nd orbit. Fig. 8 shows the Mg II line profiles at flare peak, compared with a quiescent spectra obtained at the same phase one orbital period later. Note the appearance of the Mg II 3d-3p lines at 2791.60 and 2798.82 \AA , which are not observable in the quiescent phase.

3.2.1. Temporal evolution

In Fig. 9 the fluxes integrated in the range $2798\text{--}2810 \text{ \AA}$ for the Mg II *h* line, $2788\text{--}2800 \text{ \AA}$ for the Mg II *k* line, $2780\text{--}2820 \text{ \AA}$ for the total flux, and $2738\text{--}2750 \text{ \AA}$ for the continuum are plotted versus orbital phase. The flare rises abruptly at $\phi = 0.55$ with a decay time-scale of about 6 hours. Note that both the *h* & *k* line and the continuum fluxes show similar temporal behaviours.

The Mg II fluxes measured before, during and after the flare peak are summarised in Table 4. For comparison, the quiescent fluxes obtained at the same phases in the successive orbit are reported. The relative enhancement of total Mg II lines flux, $(F_{fl} - F_q)/F_q$, is $\approx 130\%$ at flare peak and decreases to $\approx 47\%$ two hours later. The luminosity at flare-peak integrated in the $2798\text{--}2820 \text{ \AA}$ range is $1.7 \times 10^{31} \text{ erg s}^{-1}$. We estimate a flare energy output of $7.7 \times 10^{34} \text{ erg}$ from both the *h* and *k* Mg II lines. The flare energy output in 12 \AA of continuum centred at 2744 \AA is $1.4 \times 10^{34} \text{ erg}$.

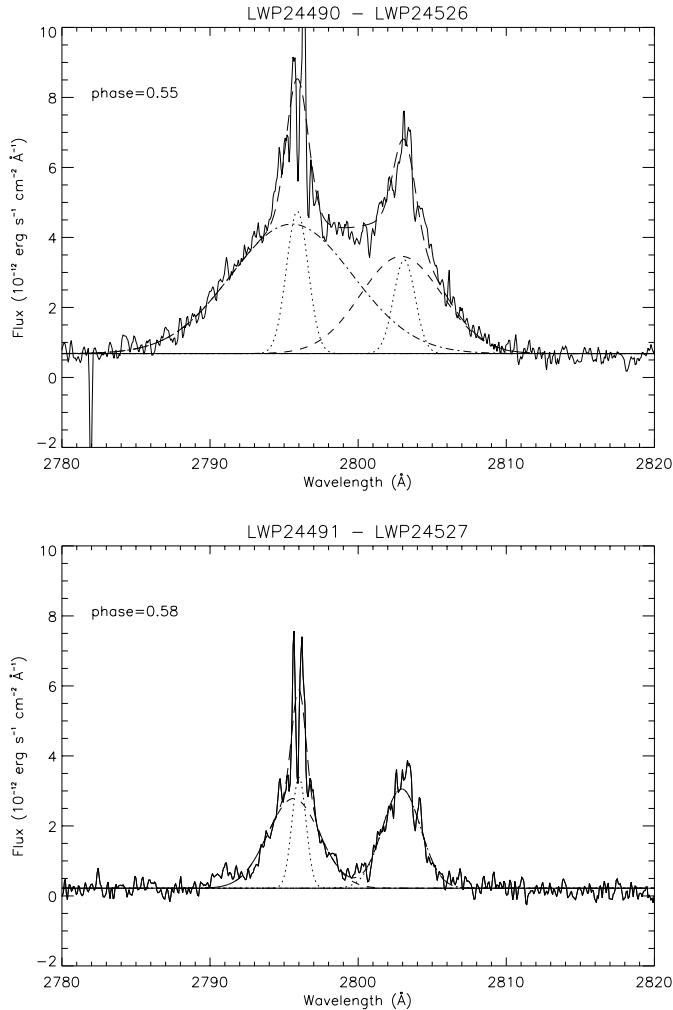
3.2.2. Flare imaging and dynamics

In order to analyse the dynamics of the pure flare event we subtracted the LWP24526 obtained at phase 0.56 during quiescence from LWP24490 obtained at phase 0.55 during the course of the flare. Four Gaussian components were necessary to fit the flare profile, one narrow (*nc*) and one broad Gaussian (*bc*) component for each of the *h* & *k* Mg II lines (see Fig. 10, upper panel). In Table 5 the resulting radial velocities with respect to the centroid

Table 4. Integrated fluxes before, during, and after the December 14 flare compared with non-flaring fluxes at the same phases, but one orbital period later.

Flare spectra			Quiescence spectra			$\frac{(F_{fl}-F_q)}{F_q}$
Image LWP	Orbital phase	Flux* erg cm ⁻² s ⁻¹	Image LWP	Orbital phase	Flux* erg cm ⁻² s ⁻¹	
24489	0.52	73.9×10^{-12}	24524	0.51	76.4×10^{-12}	≈ 0
24490	0.55	172.4×10^{-12}	24526	0.56	74.6×10^{-12}	1.31
24491	0.58	106.2×10^{-12}	24527	0.58	72.2×10^{-12}	0.47
24492	0.61	82.0×10^{-12}	comparison spectrum not available			
24494	0.67	61.5×10^{-12}	comparison spectrum not available			

* Flux integrated between 2780 and 2820 Å.

**Fig. 10.** Pure flare-peak spectrum *top panel*. Pure post-flare spectrum *bottom panel*.

of K1 star emission (v_r), the integrated flux and the FWHM of the four Gaussian components are listed (the *bc* radial velocities for *h* & *k* lines have been constrained to assume the same value. In fact the two lines form from the same ion, by the same atomic transition, i.e., in the same plasma layer and, therefore, the *h* & *k* lines must have the same radial velocity). Both narrow and broad components of the *h* & *k* Mg II lines are blue-shifted

and the broad component is more blue-shifted than the narrow component. The FWHM of these narrow and broad components are highly non-thermal suggesting an enhancement of density and/or supersonic turbulent motions of the flaring material.

The pure post-flare spectrum was obtained by subtracting the LWP24527 spectrum obtained at $\phi = 0.56$ during quiescence (3th orbit) from the LWP24491 spectrum acquired at $\phi = 0.58$ two hours after the flare peak. Also the post-flare spectrum requires a narrow and a broad Gaussian component to fit the *k* Mg II lines, while only one broad Gaussian is required for the *h* line (see Fig. 10, lower panel). Note that two hours after the flare peak the blue-shift of the broad components is still present, though less pronounced, while the narrow component (present only in the *k* line) is not blue-shifted anymore. A significant broadening is still evident at $\phi = 0.58$ for both the *nc* and the *bc* (see Table 5).

Given the geometry of the system at phase 0.55, the blue-shifts of the *bc* during and after the flare peak suggest that mass ejection occurred from the K1 towards the G5 star.

3.3. Comparison with IUESIPS processed data set

Using the same data set but reduced by the IUESIPS procedures, we find that, as for the NEWSIPS data, the Mg II *h* line profiles require a broad Gaussian component to account for their wide wings. However, this broad component appears red-shifted with respect to the K1 star at all phases (see Fig. 11). When we attempt to interpret the velocity shift variations as due to emission from a localised region we find a higher constant red-shift (about 40 km s^{-1}) (see Busà et al. 1996) than what found from the NEWSIPS processed data (10 km s^{-1}).

The different result between the NEWSIPS and IUESIPS data analysis are due to a spurious excess of red light in the IUESIPS spectra. In Fig. 12, the percent fraction of integrated flux in the red wings (with respect to the centre of mass of the binary system) for the IUESIPS and NEWSIPS are plotted. Note that the fraction of the red flux is systematically smaller in the NEWSIPS spectra, indicating that the calibration adopted in the IUESIPS considerably changes the shape of the profiles. We deduce, therefore, that analyses based upon the IUESIPS spectra are affected by systematic calibration errors.

Table 5. Parameters of the Gaussian narrow (*nc*) and broad (*bc*) components that fit the Mg II *h&k* pure flare spectra. The *bc* radial velocity for both *h* & *k* lines have been constrained to the same value.

Phase	FWHM (km s ⁻¹)		Flux*		v_r^{**} (km s ⁻¹)		FWHM (km s ⁻¹)		Flux*		v_r^{**} (km s ⁻¹)	
	nc	bc	nc	bc	nc	bc	nc	bc	nc	bc	nc	bc
	<i>k</i> line						<i>h</i> line					
0.55	182	1038	7.47	38.15	-18	-57	180	693	4.9	19.20	-13	-56
0.58	114	442	3.77	11.28	-3	-36	–	323	–	9.18	–	-38

* Flux in unit of 10^{-12} erg cm⁻² s⁻¹

** Radial velocity in the K star rest frame.

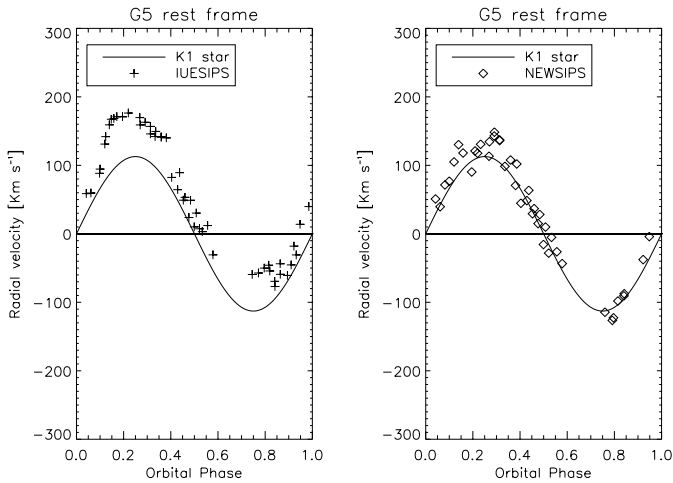


Fig. 11. Radial velocities of the active component in the rest frame of the G star. Left panel: IUESIPS processed data. Right panel: NEWSIPS processed data.

We also found that while the Mg II *k* line core was saturated in most of the IUESIPS spectra, the saturation is no more present after NEWSIPS reduction, as shown in Fig 13 where the IUESIPS and NEWSIPS LWP 24490 spectrum, that was acquired during the major flare discussed in Sect. 3.2, is shown. The increased signal-to-noise ratio and enhanced quality of the NEWSIPS data compared with the IUESIPS have been discussed by Nichols & Linsky (1996).

4. Conclusion

We have carried out Doppler Imaging analysis of IUE spectra of V 711 Tau as part of a MUSICOS campaign between 12–18 December 1992. Broad and variable extended wings were detected on the Mg II *h* line profiles at all phases and in both orbits we observed. The broad wings were successfully fitted using a broad Gaussian, which is present in all spectra and accounts for a large fraction of the flux from the global stellar Mg II *h* emission, the broad/total flux ratio being 0.36 for the K1 star. This ratio is typical for the most active stars studied by Wood et al. (1997). Our results are in general agreement with Wood et al. (1996) and Dempsey et al. (1996) analysis of GHRS spectra of V 711 Tau, but our complete phase coverage allows us to ascertain that the broad components have velocity shifts with

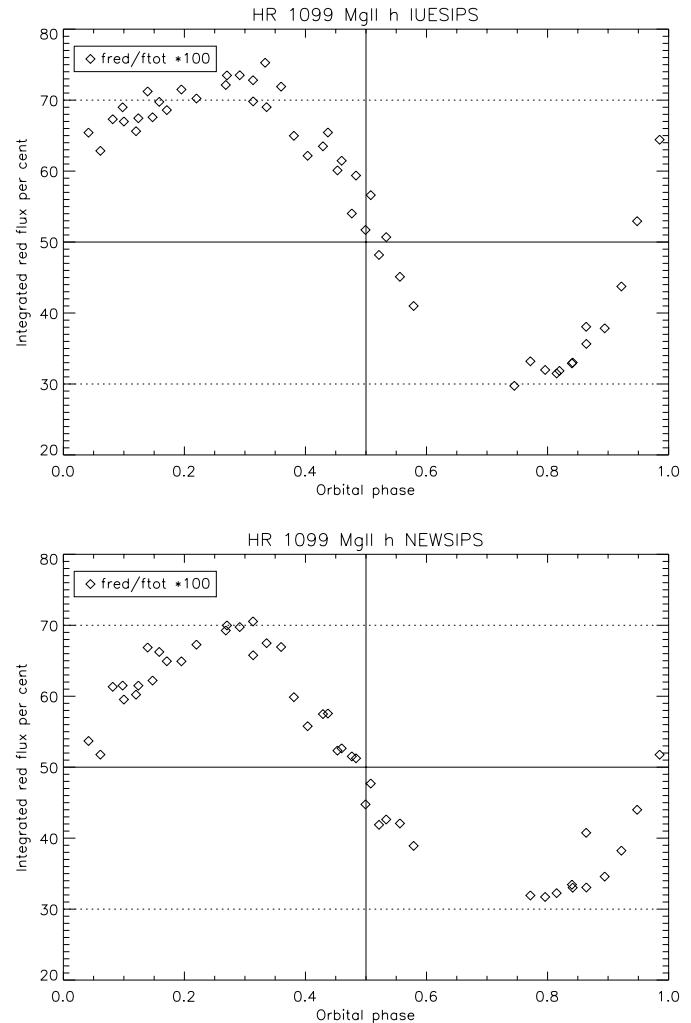


Fig. 12. Percent fraction of integrated flux in the red wing (with respect to the centre of mass of the binary system) of the Mg II *h* line of the IUESIPS (*upper panel*) and NEWSIPS profiles (*lower panel*).

respect to the K1 star that are variable in the range from -19 to +44 km s⁻¹.

Furthermore, complete phase coverage allows us to infer information of the surface structure. In particular, our analysis suggests that the broad component could represent emission that arises from a large active region close to the pole in which down-flows dominate on up-flows. If this is true the controver-

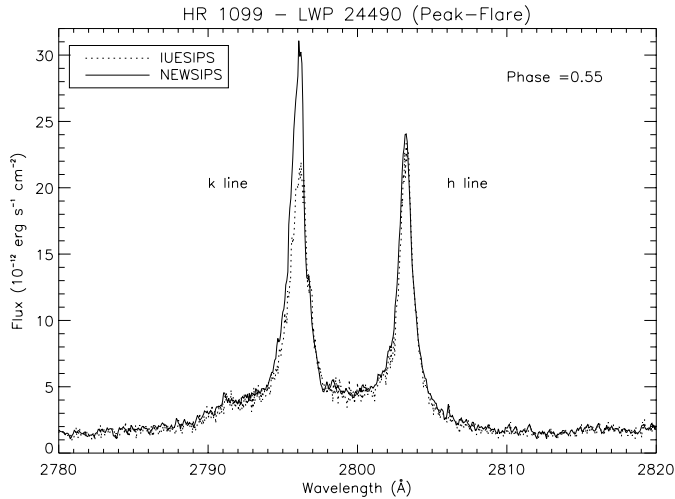


Fig. 13. Comparison between the IUESIPS and NEWSIPS LWP 24490 spectrum, acquired during the major flare discussed in Sect. 3.2. The saturation in the Mg II *k* line core in the IUESIPS data was removed by the NEWSIPS reduction. A shift of the wavelength scale was necessary to overlap the spectra because IUESIPS adopts wavelengths measured in air, while NEWSIPS adopts wavelengths measured in vacuum.

sial physical conditions that generate the broad wings of many active stars (see, e.g., Linsky et al. 1995, Wood et al. 1996), can be ascribed to localised regions rather than to the whole star.

An intra-system active region located between the two components has been revealed. This may be indicative of phenomena of mass-exchange from the K1 towards the G5 component.

The quiescent emission flux is found to be $11.1 \times 10^{-12} \text{ erg cm}^{-2} \text{ s}^{-1}$ for the K1 and $2.3 \times 10^{-12} \text{ erg cm}^{-2} \text{ s}^{-1}$ for the G5 star. The G5 Mg II *h* line flux is $\approx 6\%$ of the total Mg II *h* flux emitted from the binary system, in satisfactory agreement with the analysis of Wood et al. (1996), who found a contribution of $\approx 7.5\%$.

We estimate that the ISM in the direction of V 711 Tau has a radial velocity of $v_{IS} = 19 \pm 6 \text{ km s}^{-1}$. The equivalent width of the IS absorption line is found to be $62.3 \pm 14.0 \text{ m}\text{\AA}$.

From the spectral decomposition of spectra acquired during a major flare on December 14 we infer information on the kinematics and energetics of the flaring plasma. We find that the flare dynamics is compatible with a flaring site on the visible K1 star hemisphere with mass ejection towards the G5 companion. The emitted flux in the Mg II *h* and *k* lines was of the order of $7.7 \times 10^{34} \text{ erg}$, and the emission is characterised by a large broadening with $\text{FWHM} \approx 1000 \text{ km s}^{-1}$ at flare peak and $\text{FWHM} \approx 700 \text{ km s}^{-1}$ two hours later.

The IUESIPS MgII line profiles are affected by spurious asymmetries, that disappear in the NEWSIPS reduced spectra. A comparison between Doppler Imaging results from NEWSIPS and IUESIPS processed data shows a marked reduction of the uncertainties when using the NEWSIPS and it indicates possibly systematic errors in the wavelength calibration in the IUESIPS.

Acknowledgements. Active star research at Catania Astrophysical Observatory and the Institute of Astronomy of Catania University is funded by MURST (Ministero della Università e della Ricerca Scientifica e Tecnologica), CNAA (Consorzio Nazionale per l’Astronomia e l’Astrofisica) and the Regione Siciliana, whose financial support is gratefully acknowledged.

References

- Agrawal, P.C., Vaidya, J., 1988, MNRAS, 235, 239
 Anderson, R.C., Weiler, E.J., 1978, ApJ, 224, 143
 Ayres, T.R., 1980, The Universe at Ultraviolet Wavelengths. In: R.D. Chapman (ed.) The first two years of International Ultraviolet Explorer, NASA CP 2171, 237
 Bruls, J.H.M.J., Solanski, S.K., Schussler, M., 1998, A&A, 336, 231
 Bevington, P.R., 1969, Data Reduction and Error Analysis for the Physical Sciences, McGraw-Hill, New York.
 Busà, I., Pagano, I., Rodonò, M., Neff, J.E., 1996, “Cool Stars, Stellar System and the Sun:9”. In: Pallavicini, R. and Dupree, A.K. (eds.) Proc. of the 9th Cambridge Workshop, ASP, V.109, p.641
 Buzasi, D.L., Huenmoerder, D.P., Ramsey, L.W., 1991, PASP, 103, 1077
 Dempsey, C. R., Neff, J.E., Thorpe, M.J. et al., 1996, ApJ, 470, 1172
 Dere, K.P., Brueckner, G.E., Howard, R.A. et al., 1997, Sol. Phys., 175, 601
 Donati, J.F., Semel, M., Rees, D.E. et al., 1990, A&A, 232, L1-L4
 Donati, J.F., Brown, S.F., Semel, M. et al., 1992, A&A, 265, 682
 Dorren, J.D., Guinan, E.F., 1982, ApJ, 252, 296
 Drake, J., Brown, A., Patterer, R.J. et al., 1994, ApJ, 421, L43
 Elgarøy, Ø., Engvold, O., Jorås, P., 1997, A&A 326, 165
 Fekel, F.C., 1983, ApJ, 268, 274
 Huang, L., Zhai, D., Catala, C., Foing, B.H., 1995, “MUSICOS: Multi-Site Continuous Spectroscopy”. In: Huang, L., Zhai, D., (eds.) Proc. of the 4th MUSICOS Workshop, p. 131
 Hatzes, A.P., 1995, AJ, 109, 350
 Hatzes, A.P., 1998, A&A, 330, 541
 Linsky, J.L., Neff, J.E., Brown, A. et al., 1989, A&A, 211, 173
 Linsky, J.L., Wood, B.E., 1994, ApJ, 430, 342
 Linsky, J.L., Wood, B.E., Judge, P. et al., 1995, ApJ, 442, 381
 Neff J.E., Walter, F.M., Rodonò M., Linsky, J.L., 1989, A&A, 215, 79
 Neff J.E., Walter, F.M., Wolk, S.J., Pagano, I., 1992, AAS, 181, 6601
 Neff J.E., Pagano I., Rodonò M., 1995, “MUSICOS: Multi-Site Continuous Spectroscopy”. In: Huang, L., Zhai, D. (eds.) Proc. of the 4th MUSICOS Workshop, p. 157
 Nichols, J.S., Linsky, J.L., 1996, AJ, 111, 517
 Owen, F. N., Jones, T. W., Gibson, D. M., 1976, ApJ, 210, L27
 Pagano, I., Linsky, J.L., Carkner, L. et al., 1999, ApJ (submitted)
 Piskunov, N., Wood, B.E., Linsky et al., 1997, ApJ, 474, 315
 Robinson, R.D., Airapetian, V.S., Maran, S.P., Carpenter, K.G., 1996, ApJ, 469, 872
 Rodonò, M., Cutispoto, G., Pazzani, V. et al., 1986, A&A, 165, 135
 Rodonò, M., Byrne, P.B., Neff, J.E. et al., 1987, A&A, 176, 267
 Strassmeier, K.G., Hall, D.S., Fekel, F.C., Scheck, M., 1993, A&A, 100, 173
 Strassmeier, K.G., Rice, J.B., 1998, A&A, 339, 497
 Trigilio, C., Umana, G., Migenes, V., 1993, MNRAS, 260, 903
 Vogt, S.S., Penrod, G.D., 1983, PASP, 95, 565
 Vogt, S.S., Penrod, G.D., Hatzes, A.P., 1987, ApJ, 321, 496
 Vogt, S.S., Hatzes, A.P., Micsh, A.A., Kurster, M., 1999, ApJS, 121, 547
 Wood, B.E., Harper, G.M., Linsky, J.L., Dempsey, C. R., 1996, ApJ, 458, 761
 Wood, B.E., Linsky, J.L., Ayres, T.R. 1997, ApJ, 478, 745
 Umana, G., Trigilio, C., Tumino, M. et al., 1995, A&A, 298, 143